NJC

Accepted Manuscript

This is an *Accepted Manuscript*, which has been through the Royal Society of Chemistry peer review process and has been accepted for publication.

Accepted Manuscripts are published online shortly after acceptance, before technical editing, formatting and proof reading. Using this free service, authors can make their results available to the community, in citable form, before we publish the edited article. We will replace this *Accepted Manuscript* with the edited and formatted *Advance Article* as soon as it is available.

You can find more information about *Accepted Manuscripts* in the Information for Authors.

Please note that technical editing may introduce minor changes to the text and/or graphics, which may alter content. The journal's standard Terms & Conditions and the Ethical guidelines still apply. In no event shall the Royal Society of Chemistry be held responsible for any errors or omissions in this *Accepted Manuscript* or any consequences arising from the use of any information it contains.

ROYAL SOCIETY OF CHEMISTRY

www.rsc.org/njc

Facile synthesis of monodisperse Ag@C@Ag core–double shell spheres for application in sensing thymol and phenol simultaneously†

Tian Gan,[*ab] Zhen Lv,[a] Yaping Deng,[a] Junyong Sun,[a] Zhaoxia Shi,[a] and Yanming Liu[a]

[a] *College of Chemistry and Chemical Engineering, Xinyang Normal University, Xinyang 464000, P. R. China. E-mail: gantianxynu@163.com; Fax: +86-376-6390597; Tel.: +86-376-6390702*

[b] *State Key Laboratory of Lake Science and Environment, Nanjing Institute of Geography and Limnology, Chinese Academy of Sciences, Nanjing 210008, P. R. China*

† Electronic supplementary information (ESI) available.

A simple coupled synthesis and encapsulation route was developed to fabricate monodisperse, uniform Ag@C@Ag core–shell structured nanocomposites with excellent electrochemical and catalytic properties, in which Ag nanoparticles were firstly encapsulated in a carbonaceous shell through the catalyzed dehydration of glucose under hydrothermal condition, and the surface activated Ag@C spheres were subsequently used to accumulate $[Ag(NH_3)_2]^+$ or Ag^+ ions through electrostatic attraction to anchor Ag coating. The as–prepared nanocomposite was demonstrated to have a great potential for the simultaneous multiplexed detection of thymol and phenol, and exhibited high sensitivity and good reproducibility. In addition, the practical analytical application of the sensing platform was assessed by determination of thymol and phenol in real honey samples with satisfactory results.

Introduction

Core–shell nanostructures, constructed by cores and shells of different chemical compositions and properties, have been the subject of intensive research due to their major advantages over simple component leading to the improvement of properties such as increase in dispersibility, improved thermal and chemical stability, enhanced resistance to catalyst poisoning, increased catalytic activity, and so on.[1,2] Among them, Ag nanoparticles (NPs) based core–shell nanostructures have received significant attention.[3] For example, Ag@fullerene[4] and Ag@TiO_2[5–7] core–shell structures have shown excellent performance in plasmonic behavior and superior lithium storage, respectively. In both cases, the Ag NPs functionalize as conductive metal NPs because of their lower resistance as compared to other metal NPs.[8] However, the weak electrical conductivity as well as the nondispersibility of their coatings is not beneficial for electrochemical and biological applications. Carbon materials possess many advantages such as steady chemical properties, strong corrosion resistance, less weight and low cost,[9] which can be regarded as promising candidates to fabricate functional core–shell composite structure with metal.

Templating is the most widely used method to synthesize core–shell nanostructures. Typically, core–shell metal@carbon spheres are synthesized through multi–step synthetic procedures including metal NPs preparation, surface functionalization or modification, seeding and subsequent growing for complete carbon coating.[10] These are inherently time consuming, hence there remains a challenge to develop a simple and cost–effective process to fabricate core–shell nanostructure. One–pot approach represents a facile and green chemical strategy to simplify the synthesis process of core–shell nanostructures.[11] A recent example is the preparation of magnetic Fe_3O_4 core–carbon shell nanoparticles via the co–precipitation followed by the hydrothermal

dehydrogenation of glucose.[12] In addition, we recently reported a facile encapsulation approach to produce Fe@Fe_3C–C core–shell nanostructure using glucose as the reducer and carbon source.[13] However, one drawback of this procedure is the requirement of pre–synthesized core with suitable surface chemistry.

On the other hand, it is noticed that the chemical properties of carbon sphere are usually neglected. Liu et al have confirmed that a large number of residual hydroxyl groups lie on the surface of carbon after the hydrothermal treatment of glucose,[14] which can be ionized into negative ions in alkali environment. The negative–charged surface of carbon can be used as capturer for metal cations and another metal shell can be coated around the carbon.

Herein, on the basis of above statements and our previous studies, we designed a one–pot method for the preparation of monodispersed Ag@C spheres and their one–pot coating of another compact Ag NPs shell, where metal NPs preparation, surface modification, seeding, and the subsequent shell growing steps could be achieved in twice hydrothermal reactions. The highlights or advantages of this method could be attributed to the following two factors: (1) The Ag@C was constructed in a one–pot solvothermal synthesis to produce an Ag NP as a core and amorphous carbon with abundant dangling hydroxyl groups as the shell. This route was “green” by design as no toxic reagents were added between core and shell syntheses. (2) The Ag@C colloidal microsphere as the core template was activated all through the reaction process, which avoided prior surface modification and seeding steps naturally, thus simplified the silver coating process to a great extent. Compared with the tenuous Ag NPs on Ag/C surface in previous work by Chen et al,[15] this new configuration here could ensure the uniform and complete coverage of Ag shell on Ag@C colloidal microspheres reproducibly. Additionally, the electrochemistry experimental results

showed that these composite microspheres with Ag NP cores and Ag NP–assembled shells supported by carbon exhibited great potential for simultaneous detecting trace of thymol and phenol with very high sensitivity and satisfactory results for honey analysis.

Experimental

Chemicals and apparatus

Silver nitrate ($AgNO_3$), glucose, polyvinylpyrrolidone (PVP–K30), ammonia ($NH_3 \cdot H_2O$), thymol and phenol were purchased from Aldrich Chemicals with analytical purity. All chemicals were used as received without further purification. Thymol and phenol were dissolved into absolute ethanol to prepare standard solutions, and stored at 4 °C in dark. The water used was re–distilled.

Electrochemical measurements were performed on a CHI 660D electrochemical workstation (CH Instruments Inc. Shanghai). A conventional three–electrode system, consisting of an Ag@C@Ag modified glassy carbon electrode (GCE), a saturated calomel reference electrode (SCE) and a platinum wire auxiliary electrode, was employed. Field emission scanning electron microscopy (SEM) was conducted with a Hitachi S–4800 microscope (Japan). Field emission transmission electron microscope (TEM) images were measured using a Tecnai G220S–TWIN microscope (FEI Company, Netherlands). X–ray diffraction (XRD) pattern was recorded on a Rigaku MiniFlex600 X–ray diffractometer with Cu Kα radiation (λ = 1.5418 Å) operating at 40 kV, 15 mA. The data were collected from 5 to 80° with the scan rate of 2° min^{-1} and steps of 0.02°. UV–vis absorption spectrum was recorded on a UV–vis 2550 spectroscope (Shimadzu, Ltd., Tokyo, Japan). Fourier transform infrared (FTIR)

measurements (Perkin Elmer FT–IR spectrophotometer) were collected in the spectral range of 400–4000 cm^{-1} with a resolution better than 0.1 cm^{-1}.

Liquid chromatography (LC) detection of thymol and phenol was carried out with Agilent 1100, coupled with a fluorescence detector.[16] The Discovery RP–AmideC_{16} analytical column (150 mm×4.6 mm) was used. The mobile phase was acetonitrile and water mixture, filtered through 0.45–μm Millipore filter prior to use. The elution was programmed with an initial isocratic step with a 20/80 (v/v) acetonitrile/water mixture for 3 min, a gradient to 40/60 (v/v) acetonitrile/water in 0.01 min, and then, maintaining this mixture for 8 min. The initial conditions were finally re–established in 1 min and held for 15 min. The flow–rate was 1 mL min^{-1}. And the sample injection volume was 100 μL. The detection was operated at wavelengths of 274/590 nm (excitation and emission).

Synthesis of Ag@C@Ag

The core–shell structured Ag@C spheres were synthesized by hydrothermal method modified from previous report.[17] In a typical synthesis, 0.0102 g of $AgNO_3$ and 3.4230 g of glucose were respectively dissolved in 2 mL and 38 mL of distilled water under vigorous stirring. When the two kinds of solution were fully mixed, the resultant mixture was placed in a 50 mL Teflon–lined stainless steel autoclave and heated at 180 °C for 4 h. The black products were then collected, washed five times with water and ethanol, and dried at 80 °C for 5 h.

In order to coat Ag@C with Ag NPs, PVP was used as weak reducer.[18] 0.03125 g of Ag@C, 33.75 mL of ethanol and 2.5 g of PVP–K30 were mixed step–by–step under vigorous stirring in a reagent bottle. To the homogeneous solution obtained, 5 mL re–distilled water containing 0.25 g of $AgNO_3$ and 0.4 mL $NH_3 \cdot H_2O$ was added and

allowed to stir for another 10 min. After further dispersion in an ultrasonic bath for 10 min, the resultant dark transparent solution was then transferred to a 50 mL Teflon–lined stainless steel autoclave, tightly sealed and heated at a temperature of 120 °C for 6 h. After the reaction is complete, the autoclave was allowed to cool to room temperature and the resultant precipitate was centrifuged and washed completely with water and ethanol. The powder sample obtained was air–dried at 50 °C.

For comparison, carbon spheres (CS) without the Ag core were also prepared according to the procedure for Ag@C, but exclude the addition of $AgNO_3$.

Electrode preparation

Firstly, a 20.0–mg Ag@C@Ag was dispersed into 10.0 mL of re–distilled water by 1–h ultrasonic agitation to give a homogeneous Ag@C@Ag suspension. Secondly, the GCE (diameter of 3 mm) was polished with 0.05 μm alumina slurry on silk, and then washed with ethanol/water (1:1, v/v) and water in an ultrasonic bath, each for 1 min. 10.0 μL of the obtained Ag@C@Ag solution was coated onto the surface of GCE and allowed to dry under an infrared lamp in the air.

Similarly, the CS film–modified GCE was prepared by coating 10.0 μL of 2.0 mg mL^{-1} CS suspension on GCE surface. And the Ag@C film–modified GCE was prepared by coating 10.0 μL of 2.0 mg mL^{-1} Ag@C suspension on GCE surface.

Analytical procedure

Unless otherwise stated, 0.1 M H_2SO_4 was used as determining medium for thymol and phenol analysis. The analytical procedure mainly contains two steps: accumulation step and determining step. Firstly, thymol and phenol were

preconcentrated onto the Ag@C@Ag film–modified GCE surface under open–circuit for 60–s stirring. After that, the differential pulse voltammograms from 0.5 to 1.3 V were recorded, and the oxidation peak currents at 0.86 V and 1.03 V were measured as the analytical signals for thymol and phenol, respectively.

Results and discussion

Characterizations

The dispersibility and stability of CS, Ag@C and Ag@C@Ag in water were tested (Fig. 1). It can be seen that all of these three materials can be dispersed into water due to the oxygen–containing groups on carbon surface that formed during the carbonization of glucose.[14] The color of Ag@C suspension is much similar to that of CS because the Ag NPs are encapsulated into carbon shell, so both show the characteristic appearance of CS. However, with the in situ growth of Ag NPs on carbon surface, the color changes from yellowish–brown to black, indicating the coating of another shell outside of carbon.

The crystalline structures of the prepared materials were studied by XRD (Fig. 1). In XRD pattern of CS (curve a), the broad peak in the 2θ range of 10–30° is attributed to the amorphous carbon.[19] In contrast, four new diffraction peaks at 2θ = 38.1°, 44.2°, 64.5° and 77.3° appear on Ag@C (curve b) represent the (111), (200), (220) and (311) planes of the face–centered–cubic structure of metallic Ag, respectively (JCPDS 870597). Furthermore, the diffraction peak corresponding to amorphous carbon still exists. Therefore, Ag NP coexists with carbon in this hybrid. After the further coating of Ag NPs (curve c), the intensity of diffraction peaks from Ag enhances significantly, demonstrating an increasing amount of Ag crystals. Only diffraction peaks of the Ag

appear and there is almost no carbon diffraction peak anymore, which indicate that the Ag NPs successfully and densely deposit on the surface of carbon.[20] According to the Scherrer formula, the diameters of Ag NPs corresponding to inner core and outer shell are respectively calculated to be 35.7 and 25.6 nm, which means that the encapsulated and coated Ag are in nanoscale.

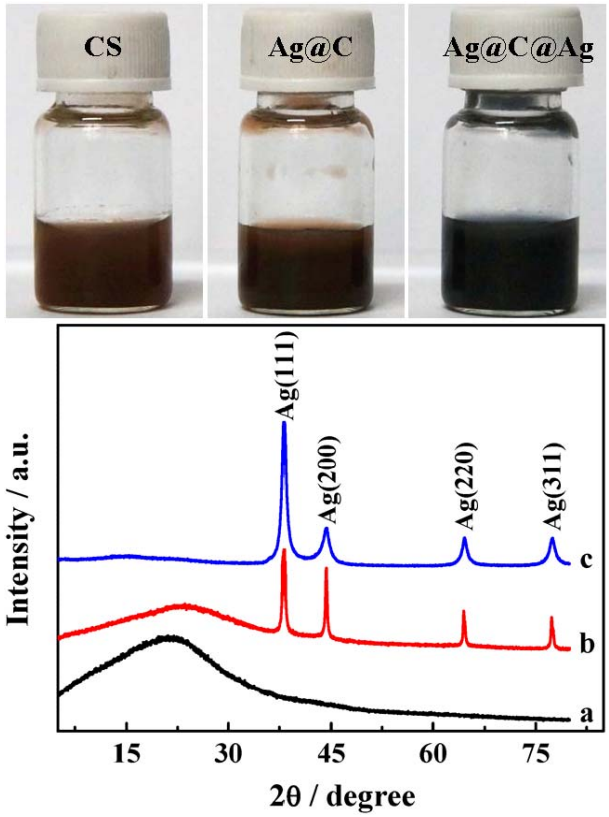

Fig. 1 Appearance and XRD pattern of CS (a), Ag@C (b) and Ag@C@Ag (c).

The formation of core–shell structured Ag@C@Ag spheres was also observed from SEM and TEM images. The SEM study depicted in Fig. 2a indicates that the morphology of hydrothermally grown Ag@C is sphere shaped. Fig. 2d shows typical TEM image of Ag@C spheres with an average diameter of about 228 nm, with smooth surfaces. It seems that most spheres exhibit perfect core–shell nanostructures with single Ag core (~36 nm) and uniform shell thickness (~95 nm). Figs. 2b, c, e and f show the SEM and TEM images of Ag coated Ag@C. Low–magnification SEM

image of Ag@C@Ag nanocomposite is illustrated in Fig. 2b, where Ag@C spheres are uniformly coated with Ag NPs. The uniform coating is basically composed of a large number of spherical Ag NPs with different sizes, ranging from 20 to 30 nm. The average diameter of the Ag NP is about 26 nm, which is in agreement with the above XRD observation. High–magnification SEM image shows that the surface of the Ag@C sphere becomes rough after the growth of Ag NPs shell (Fig. 2c), and the Ag@C spheres are covered with Ag NPs completely, which indicates the excellent interfacial interaction between carbon and Ag NPs. The TEM image shown in Fig. 2e further confirms the shell growth of Ag NPs. The apparent contrast in the TEM image between Ag@C core and Ag NPs shell offers evidence for the formation of Ag@C@Ag spheres. The periodicity of the lattice fringes for Ag obtained from high resolution–TEM image of Ag@C@Ag indicates that d = 0.236 nm (Fig. 2f), corresponding to the (111) planes of the metallic Ag with face–centered–cubic structure.[21]

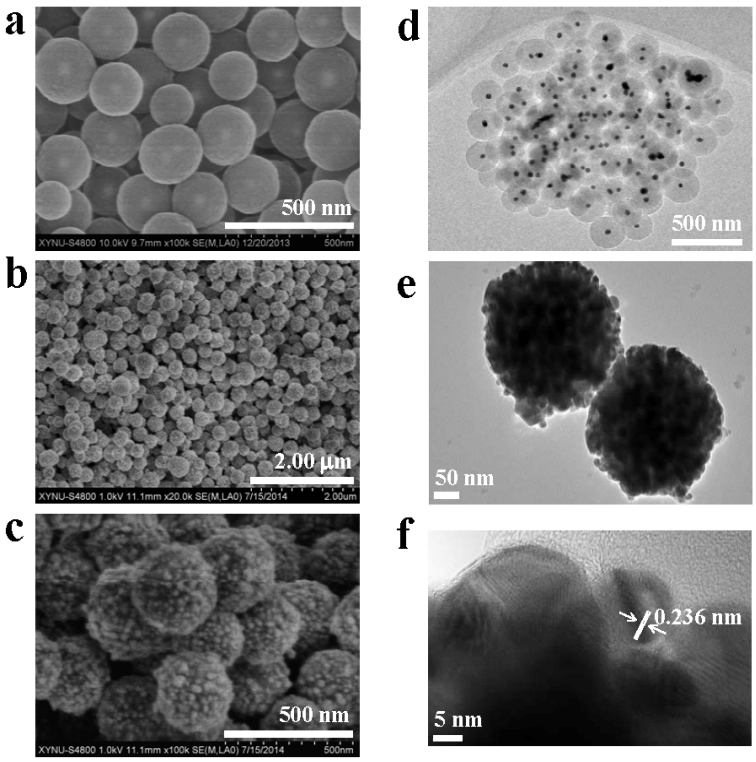

Fig. 2 SEM (a–c) and TEM (d–f) images of Ag@C (a, d) and Ag@C@Ag (b, c, e, f).

A UV–vis spectrum study of Ag@C@Ag was further performed (Fig. 3A). The extinction peak corresponding to typical extinction spectrum of Ag NPs red–shifts to 460 nm, this is resulted from the coverage of Ag NPs by carbonaceous shells.[20] Furthermore, the absorption in a wide range from 200 to 600 nm is generated from the intermediary carbonaceous shell.

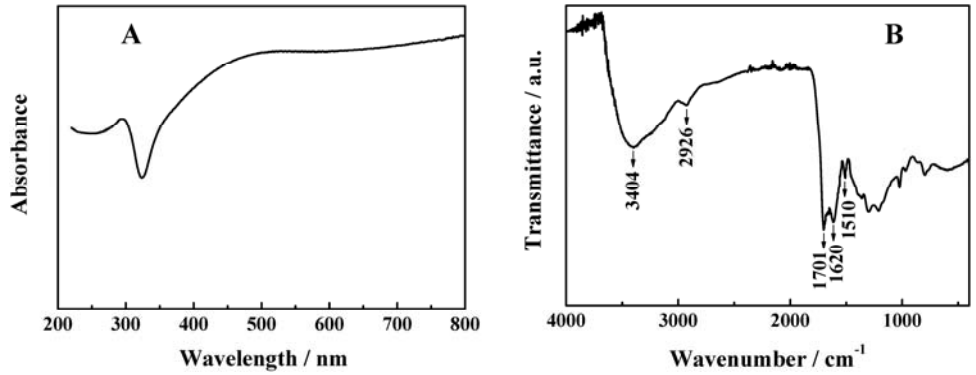

Fig. 3 (A) UV–vis spectrum of Ag@C@Ag. (B) FTIR spectrum of Ag@C.

Growth mechanism of Ag@C@Ag core–double shell spheres

The schematic illustration in Scheme 1 depicts the growth process of Ag@C@Ag core–double shell spheres: Firstly, nucleation of inner Ag NPs (step a). After being heated to 180 °C in autoclaves, Ag^{+} will be deoxidized by glucose in their homogeneous mixed solution, and then Ag NPs nucleate gradually. Secondly, growth of carbonaceous shell (step b). The small satellite Ag NPs are evenly dispersed in solution, while exposing reactive surfaces outside, which catalyze following carbonization of glucose and lead to in situ deposition of carbonaceous products around the Ag NP surfaces to form carbonaceous shells. The FTIR spectrum (Fig. 3B) clearly shows that a large amount of functional groups such as –C–O (1000–1450 cm^{-1}), –OH (1000–1450 cm^{-1}), C=O (1701 cm^{-1}), C=C (1620 and 1510 cm^{-1}), C–H (2926 cm^{-1}) and O–H (3404 cm^{-1}) covalently bond onto the carbon framework in the carbonaceous component. These surface functional groups can be broken or form

ionized sites (O^- groups) by hydroxyl anions present in alkaline conditions, which imply that a large surface charge will be present. Consequently, positive–charged complex ions $[Ag(NH_3)_2]^+$ or Ag^+ will be accumulated around the Ag@C microspheres through electrostatic attraction. Thirdly, seeding of outer Ag NPs (step c). The captured $[Ag(NH_3)_2]^+$ or Ag^+ are gradually deoxidized by PVP as gentle reducer, and Ag NPs are formed in situ as seeds. Finally, growth of Ag shell (step d). The initial–formed Ag seeds can act as growing centers for the subsequent shell growth until complete Ag coverage is realized. All the reaction steps mentioned above are integrated and achieved in two–step hydrothermal reaction in our work.

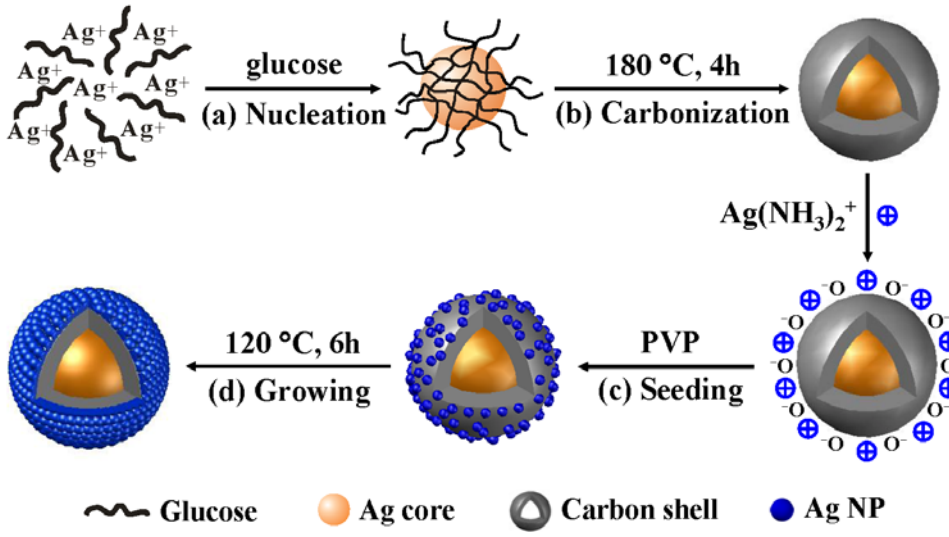

Scheme 1 Schematic illustration of the formation of core–shell structured Ag@C@Ag spheres.

Voltammetric behaviors of thymol and phenol

The electrochemical behaviors of thymol and phenol at the bare GCE and Ag@C@Ag film–modified GCE were investigated using cyclic voltammetry (CV). Fig. 4a shows the cyclic voltammograms of 0.1 mM thymol on the bare GCE at scan rate of 100 mV s^{-1}. In 0.1 M H_2SO_4, an oxidation peak is observed at 0.98 V during the anodic sweep

from 0.5 to 1.3 V. On the following reverse scan, no corresponding reduction peak is observed, suggesting that the electrochemical oxidation of thymol on the bare GCE is irreversible. The cyclic voltammogram of Ag@C@Ag film–modified GCE in 0.1 mM thymol is depicted as Fig. 4b. During the anodic potential sweep, a well–defined and sensitive oxidation peak appears at 0.95 V. On the reverse scan, a negligible reduction peak is observed at 0.83 V. From the comparison between curves (a) and (b), it is very clear that the oxidation peak current of thymol obviously increases at the Ag@C@Ag film–modified GCE. This can be attributed to the following two reasons: on one hand, the carbon shell outside effectively protects the Ag NPs from corrosion. On the other hand, the core–shell architecture maximizes the Ag–support interaction through the three–dimensional contact between the Ag NPs and the carbon, thereby facilitating the electron transfer rate.

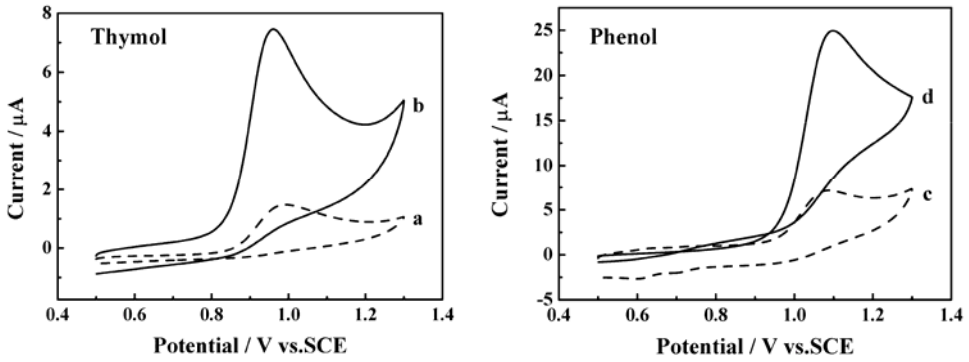

Fig. 4 Cyclic voltammograms of 0.1 mM thymol and phenol at bare GCE (a,c) and Ag@C@Ag/GCE (b,d) in 0.1 M H_2SO_4. Scan rate: 100 mV s^{-1}.

The effectiveness of Ag@C@Ag film–modified GCE for the oxidation of phenol was also assessed by CV in 0.1 M H_2SO_4. Compared with bare GCE (Fig. 4c), sharp and well–resolved oxidation peak of phenol is found on the Ag@C@Ag film–modified GCE (Fig. 4d), suggesting that the Ag@C@Ag has a strong enhancement ability for the electric signal of phenol. The electrochemical reaction of

phenol on the Ag@C@Ag film–modified GCE is a totally irreversible process. Ag@C@Ag can be used for the simultaneous determination of thymol and phenol because this nanocomposite has the ability to enhance the determination sensitivity of thymol and phenol.

The electrochemical responses of low concentration of thymol and phenol on the surface of bare GCE, CS/GCE, Ag@C/GCE and Ag@C@Ag/GCE were compared using differential pulse voltammetry (DPV). As seen in Fig. 5, two oxidation peaks at 0.85 V (O1) and 0.99 V (O2) corresponding to thymol and phenol are observed on the bare GCE surface, and the peak currents are relatively low (curve a). The weak response signals suggest that the oxidation activities of thymol and phenol on bare GCE surface are low. Under the identical conditions, the oxidation peak currents increase at the CS film–coated GCE (curve b). CS with good electric conductivity can form a perfect thin film on GCE surface. Therefore, the CS film–coated GCE has better conductivity and exhibits higher accumulation ability to thymol and phenol. Without a doubt, the oxidation peak currents of thymol and phenol increase at the CS film–coated GCE. For the Ag@C/GCE, the presence of Ag core leads to the augmented current responses of thymol and phenol (curve c). This indicates better electrocatalytic oxidation of thymol and phenol by the Ag NPs. In comparison with the Ag@C/GCE, thymol and phenol at the Ag@C@Ag/GCE exhibit more sensitive electrochemical responses (curve d). The obvious peak current enlargements indicate that Ag@C@Ag exhibit strong signal enhancement for the oxidation of thymol and phenol. SEM and TEM measurements tell us that the obtained Ag@C@Ag samples possess excellent monodispersity, rough and textured surfaces. As a result, the accumulation efficiency is improved remarkably, and the oxidation signals enhance greatly. In addition, the DPV response of Ag@C@Ag/GCE in the absence of thymol

and phenol is also studied, and the curve is shown as curve e. It is virtually featureless and no oxidation wave appears. So the observed oxidation peak at 0.86 and 1.03 V are attributed to the oxidation of thymol and phenol. In summary, the prepared Ag@C@Ag spheres are more active and greatly increase the detection sensitivity of thymol and phenol.

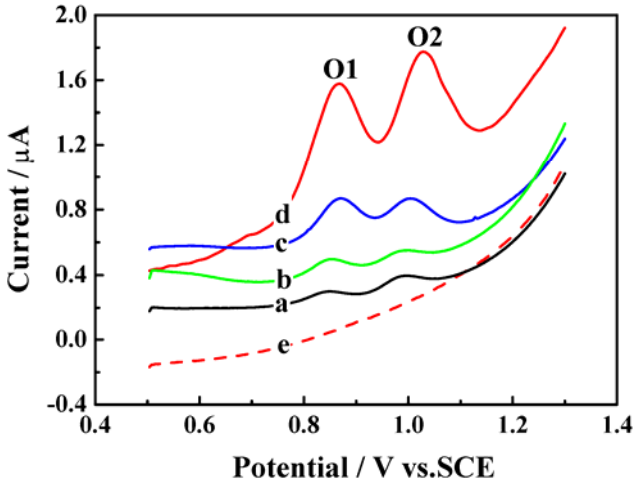

Fig. 5 DPV graphs of bare GCE (a), CS/GCE (b), Ag@C/GCE (c) and Ag@C@Ag/GCE (d) in 0.1 M H_2SO_4 containing 1.0 μM thymol and 5.0 μM phenol. Curve e corresponds to DP voltammogram of Ag@C@Ag/GCE in blank solution. Accumulation time = 60 s, pulse amplitude = 50 mV, pulse width = 0.2 s, pulse period = 0.5 s.

Effect of scan rate

The influences of scan rate on electrochemical behaviors of 0.1 mM thymol and phenol at the Ag@C@Ag/GCE in 0.1 M H_2SO_4 were also investigated (Fig. 6). Good linearity between the anodic peak current (I_p) and the scan rate (v) with $r^2 = 0.994$ and $r^2 = 0.995$ are obtained within the range from 50 to 300 mV s^{-1} for thymol (inset A of Fig. 6) and phenol (inset B of Fig. 6), respectively. The linear regression equations can be expressed as I_p (μA) = –1.111+0.0803 v (mV s^{-1}) (for thymol) and I_p (μA) =

299 7.307+0.173 v (mV s^{-1}) (for phenol). The results indicate that the electrochemical
300 oxidation of thymol and phenol at the Ag@C@Ag/GCE are adsorption–controlled
301 processes. The peak potentials (E_p) of thymol and phenol shift to more positive values
302 with the increase of scan rate, which further indicates the irreversibility of the
303 oxidation processes.

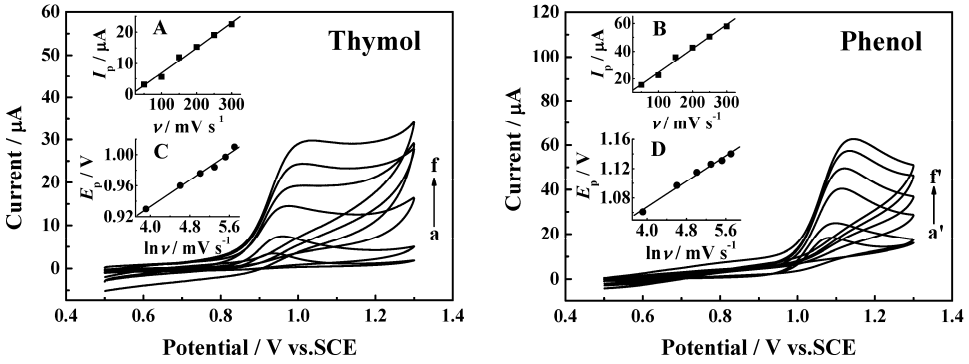

304

305 **Fig. 6** Cyclic voltammograms of 0.1 mM thymol and phenol in 0.1 M H_2SO_4 at the
306 Ag@C@Ag/GCE with different scan rates including 50 (a,a′), 100 (b,b′), 150 (c,c′),
307 200 (d,d′), 250 (e,e′) and 300 (f,f′) mV s^{-1}. Inset: linear relationship of I_p vs. v (A,B)
308 and E_p vs. ln$v$ (C,D).

309

310 For an irreversible and adsorption–controlled oxidation process, the relationship
311 between E_p and v is defined by the following equation according to Laviron′s theory:[22]

312 $$E_p = E^{0'} + \frac{RT}{\alpha nF}\ln\frac{RTk^0}{\alpha nF} + \frac{RT}{\alpha nF}\ln\nu \qquad (1)$$

313 where $E^{0'}$ is the formal potential, k^0 is the standard heterogeneous electron transfer
314 rate constant, T is the temperature, F is the Faraday constant, α is the electron transfer
315 coefficient, and n is the number of transferred electrons. In this work, the E_p of thymol
316 and phenol against logarithm of scan rate (ln$v$) is also examined under the same
317 conditions and show linear relationships (insets C and D of Fig. 6), following the
318 regression equations:

$E_p = 0.762+0.0426 \ln v$, $r^2 = 0.995$ (thymol)

$E_p = 0.894+0.0434 \ln v$, $r^2 = 0.995$ (phenol)

Combining equation (1), we can calculate the value of αn to be 0.603 and 0.592 for thymol and phenol, respectively. And the calculation has been given in details in ESI†. Generally, α is assumed as 0.5 for a totally irreversible electrode process. Hence one electron is involved in the oxidation of thymol and phenol, which is consistent with the reported results.[23,24] The oxidation mechanisms for thymol and phenol on Ag@C@Ag film modified GCE are presented in Scheme 2.

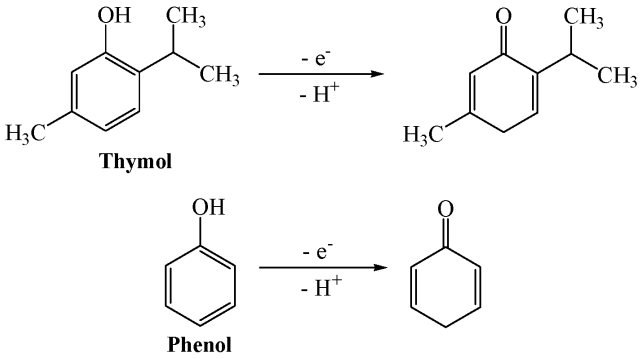

Scheme 2 Electrochemical reaction mechanisms of thymol and phenol.

Optimization of experimental conditions

The effects of several parameters, such as the electrolyte, amount of Ag@C@Ag suspension, accumulation potential and time on the voltammetric responses of thymol and phenol using this method were investigated.

The electrochemical responses of 1.0 μM thymol and phenol at the Ag@C@Ag film modified electrode in different supporting electrolytes such as 0.2 M disodium hydrogen phosphate–citric acid buffer (pH 2.2–8.0), 0.2 M acetic acid–sodium acetate buffer (pH 2.6–5.8), 0.2 M boric acid–borax buffer (pH 7.4–9.0), 0.1 M disodium hydrogen phosphate–sodium dihydrogen phosphate buffer (pH 5.8–8.0), Britton–Robinson buffer (pH 1.81–11.92) and 0.1 M HCl, H_2SO_4, $HClO_4$, NaOH

339 solutions were examined by DPV. In alkaline electrolytes, the Ag NPs on Ag@C
340 microspheres will react with OH^- and the final products Ag_2O can be formed. So the
341 electrochemical activity of the modified electrode is weakened seriously and no redox
342 peaks attributing to thymol and phenol can be observed. However, two small
343 oxidation peaks are found in neutral and weak acid environment. But evident peaks
344 can be obtained in strong acid solutions, like 0.1 M HCl, H_2SO_4, and $HClO_4$, and the
345 best voltammogram shape in 0.1 M H_2SO_4. Therefore, 0.1 M H_2SO_4 was selected as
346 the electrocatalytic medium for the simultaneous determination of thymol and phenol.
347 It is well clear that Ag@C@Ag spheres can remarkably improve the oxidation peak
348 current of thymol and phenol from Fig. 4 and Fig. 5. However, the electron transfer
349 will be blocked and the background current may increase if the modifier film is too
350 thick on electrode surface. The experimental results show that as gradually improving
351 the amount of Ag@C@Ag suspension from 0 to 10 μL, the oxidation peak currents of
352 thymol and phenol increase dramatically because the sites for adsorption of thymol
353 and phenol also increase, resulting in much higher accumulation efficiency, and thus
354 the obvious enhancement of oxidation peak current. However, the oxidation peak
355 current of thymol and phenol decrease when the amount of Ag@C@Ag suspension on
356 electrode surface exceeds 10 μL, and the very thick film tends to fall off the electrode
357 surface when dipped in electrolyte. In this work, the optimized amount of Ag@C@Ag
358 suspension was chosen as 10 μL.
359 The effects of accumulation potential and time on the anodic peak currents of 1.0
360 μM thymol and phenol were examined by DPV. The effects of accumulation potential
361 on the responses of thymol and phenol were investigated under different potentials.
362 The accumulation time was 2 min, and the studied accumulation potential changed
363 from 0.1 to 0.7 V. Moreover, the accumulation step was also conducted under

open–circuit. It is found that the oxidation peak current of 1.0 μM thymol and phenol almost keep unchanged, indicating no influence of accumulation potential on the detection of thymol and phenol. Herein, the accumulation step was performed under open–circuit.

The influence of accumulation time on the oxidation peak currents of thymol and phenol was also evaluated. The oxidation peak currents increase with the accumulation time increase, and when the accumulation time is longer than 60 s, the peak currents converge to a stable value, indicating that the absorption of thymol and phenol onto the Ag@C@Ag film has reached saturation quickly. Therefore, the accumulation time was set to 60 s.

Reproducibility and Interference

After each measurement, the Ag@C@Ag film was carefully removed from the GCE surface and another new Ag@C@Ag modified GCE was remade as above–mentioned procedure. The reproducibility between multiple Ag@C@Ag modified electrodes was estimated by comparing the oxidation peak currents of 1.0 μM thymol and phenol. The relative standard deviation (RSD) on ten Ag@C@Ag modified GCEs is 3.7% and 4.2% for thymol and phenol, respectively, revealing that this method possesses good reproducibility.

The interferences of many foreign species (especially contained in honey sample) on the determination of thymol and phenol were studied by DPV under the above–optimized conditions. The oxidation peak currents of 1.0 μM thymol and phenol in the absence and presence of foreign species with various concentrations were measured, respectively. Based on this, the peak current change can be achieved. Herein, when the peak current change exceeds 8%, it is considered that this substance

388 causes obvious interference, and the corresponding concentration is defined as
389 tolerance level. The results are listed in Table 1, suggesting that 5000–fold
390 concentration of Al^{3+}, 1000–fold concentration of Cu^{2+}, NO_3^-, K^+, Na^+, Ca^{2+}, Zn^{2+},
391 Mg^{2+}, H_2O_2, glucose, 500–fold concentration of tartrazine, 250–fold concentration of
392 ascorbic acid, and 50–fold concentration of hydroquinone almost have no influence
393 on the determination of thymol and phenol.

394 Table 1 Interference on the determination of 1.0 μM thymol and phenol

Interferents	Tolerance level (M)	Signal change for thymol (%)	Signal change for phenol (%)
Al^{3+}	5.00×10^{-3}	3.5	0.95
Cu^{2+}	1.00×10^{-3}	–6.4	–2.6
NO_3^-	1.00×10^{-3}	5.1	8.0
K^+	1.00×10^{-3}	5.0	7.6
Na^+	1.00×10^{-3}	7.0	–3.1
Ca^{2+}	1.00×10^{-3}	–4.5	–6.7
Zn^{2+}	1.00×10^{-3}	–1.7	–5.0
Mg^{2+}	1.00×10^{-3}	7.5	1.3
H_2O_2	1.00×10^{-3}	0.8	–4.6
Glucose	1.00×10^{-3}	1.2	7.2
Tartrazine	5.00×10^{-4}	–6.2	–5.5
Ascorbic acid	2.50×10^{-4}	–7.3	1.8
Hydroquinone	5.00×10^{-5}	3.9	3.4

395 **Simultaneous determination of thymol and phenol**

396 For simultaneous and quantitative determination of thymol and phenol, DPV curves at

different concentrations of thymol were recorded in Fig. 7A, where phenol concentration was kept at 3.0 μM. The inset shows that the peak current varies linearly with thymol concentration between 0.1 and 10 μM with r = 0.997. Importantly, the anodic peak current of phenol is almost uninfluenced by the increase of thymol concentration, suggesting that oxidation of thymol and phenol at the Ag@C@Ag/GCE is independent of each other. With the DPV technique the detection limit of thymol is 21.6 nM in the presence of 3.0 μM phenol interference (S/N = 3). Fig. 7B presents DPV responses at different concentrations of phenol while thymol is kept constant at 1.0 μM. Similar to the scenario in Fig. 7A, the anodic peak current of thymol stays almost constant as phenol concentration is increased gradually, further confirming that this modified electrode can be employed for simultaneous determination of thymol and phenol. The inset in Fig. 7B illustrates that the peak current increases linearly with phenol concentration between 0.5 and 50 μM with r = 0.999. In the presence of thymol, the low detection limit is 41.5 nM for phenol (S/N = 3).

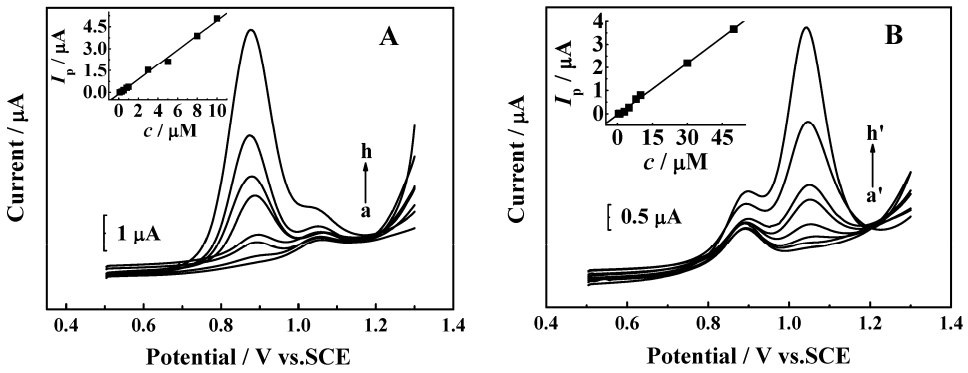

Fig. 7 DPVs of Ag@C@Ag/GCE in (A) 3.5 μM phenol and different concentration of thymol: 0.1, 0.3, 0.5, 0.8, 1.0, 3.0, 5.0, 8.0 and 10 μM (from a to h), and (B) 1.0 μM phenol and different concentration of phenol: 0.5, 0.8, 1.0, 3.0, 5.0, 8.0, 10, 30 and 50 μM (from a′ to h′). The insets show the calibration plots of thymol and phenol versus

417 peak current. Other conditions are as in Fig. 5.

418

419 Although a lot of electrochemical methods have been reported for the detection of
420 thymol or phenol,[23–27] but none of them intends to analysis thymol and phenol
421 simultaneously. It is significant that Ag@C@Ag core–shell structured spheres used in
422 our study can realize the direct and simultaneous determination of thymol and phenol
423 with much lower detection limits (Table 2). Moreover, this is the first report for the
424 simultaneous determination of thymol and phenol based on electrochemical method as
425 far as we know.

426 Table 2 Comparison of the analytical performances of this work with the reports

Modified electrode	Analyte	Linear range (μM)	Limit of detection (nM)	Reference
CeO_2/graphene/GCE	Thymol	0.1~18	50	23
Graphene oxide/GCE	Thymol	2~200	65	25
Zincon/CPE	Phenol	21~292 and 357~922	900	24
ZnO/CNTs[a]/HPDB[b]/CPE[c]	Phenol	1.0~750	500	26
Poly diphenylamine/CNTs/GCE	Phenol	9.8~80	500	27
Ag@C@Ag/GCE	Thymol	0.1~10	21.6	This work
	Phenol	0.5~50	41.5	

427 [a] CNT: Carbon nanotube

428 [b] HPDB: N-(4-hydroxyphenyl)-3,5-dinitrobenzamide

429 [c] CPE: carbon paste electrode

Honey samples analysis

Honey is a naturally sweet and levorotatory carbohydrate rich product, which is elaborated by honey bees from carbohydrate–containing exudates produced by plants, and is largely consumed worldwide.[28] According to EC norm 2001/110/EC (2002), honey must be exempt of antibiotics, pesticides, atmospheric pollutants and heavy metals. However, thymol and phenol can usually be found in honey as residues of acaricide against Varroa destructor[29] and bee repellent,[30] respectively. Although thymol residues in honey are not toxic, they can devalue honey quality.[24] Contrarily, phenol is known have adverse effects.[31] Therefore, this newly–proposed method was used to detect thymol and phenol in honey samples of different botanical origin (chrysanthemum, jujube flower and Chinese milk velch) to evaluate its application in the food control sciences. These honey samples were obtained from several beekeepers from China. All samples were kept sealed in the absence of light. Next, 1.00 g of each honey sample was exactly weighed and respectively dissolved into 10 mL hot water with a temperature of about 50 °C, and then 500 μL of the completely dissolved sample solution was added into 0.1 M H_2SO_4, and then analyzed according to the above–described procedure under the optimized conditions. Table 3 shows the content of thymol and phenol in three honey samples, which is measured by the standard addition method. Each sample undergoes six parallel measurements, and the RSD is below 3%, suggesting that this method possesses good reproducibility. To testify the accuracy of this method, the LC was also used to determine thymol and phenol. The results are listed in Table 2, too. It is found that the results by Ag@C@Ag film modified GCE and LC are in good agreement, indicative of good accuracy. Otherwise, the recoveries of thymol and phenol standard that added into the samples are also measured, and the results are in the range from 96.4% to 107%, indicating

that this method has great potential in the practical sample analysis.

Table 3 Detection of thymol and phenol in Chrysanthemum honey (A), Jujube flower honey (B) and Chinese milk velch honey (C) samples

Sample	Analyte	Ag@C@Ag/GCE (μM)	RSD (%)	LC (μM)	Rel error (%)	Added (μM)	Found (μM)	Recovery (%)
A	thymol	/		/		2.00	2.11	105
	phenol	0.0831	2.9	0.0802	3.62	1.00	0.964	96.4
B	thymol	0.400	1.7	0.414	–3.38	0.500	0.531	106
	phenol	/		/		0.800	0.845	106
C	thymol	0.320	2.3	0.309	3.56	0.600	0.588	98.0
	phenol	/		/		1.00	1.07	107

Conclusion

In summary, we have successfully developed a facile one–pot approach to produce uniform Ag@carbon with a core–shell structure by combining simultaneous Ag reduction and carbonization of glucose. Subsequently, a template–activated strategy toward uniform coating Ag nanoparticles on the Ag@carbon microspheres in one step was presented, which greatly simplified the traditional coating process and may provide a simple avenue for other metal encapsulation and coating. The uniform Ag@carbon@Ag core–shell composite microspheres were also investigated as electrochemical platform, which demonstrated an excellent detecting performance to thymol and phenol. Armed with the remarkable advantages, such as facile one–pot

synthesis, low analyte consumption, inexpensive cost and fast response time, the electrochemical sensing platform may hold great potential for the in–field food safety monitoring.

Acknowledgment

The authors acknowledge funding support from the National Natural Science Foundation of China (No. 61201091) and the open fund of State Key Laboratory of Lake Science and Environment (No. 2014SKL013).

References

1 P. Melinon, S. Begin–Colin, J. L. Duvail, F. Gauffre, N. H. Boime, G. Ledoux, J. Plain, P. Reiss, F. Silly and B. Warot–Fonrose, *Phys. Rep.–Rev. Sec. Phys. Lett.*, 2014, 543, 163–197.

2 S. Dutt, P. F. Siril, V. Sharma and S. Periasamy, *New J. Chem.*, 2015, 39, 902–908.

3 A. Monga and B. Pal, *New J. Chem.*, 2015, 39, 304–313.

4 R. Singhal, D. C. Agarwal, S. Mohapatra, Y. K. Mishra, D. Kabiraj, F. Singh, D. K. Avasthi, A. K. Chawla, R. Chandra, G. Mattei and J. C. Pivin, *Appl. Phys. Lett.*, 2008, 93, 103114.

5 V. S. K. Chakravadhanula, Y. K. Mishra, V. G. Kotnur, D. K. Avasthi, T. Strunskus, V. Zaporotchenko, D. Fink, L. Kienle and F. Faupel, *Beilstein J. Nanotechnol.*, 2014, 5, 1419–1431.

6 S. Mohapatra, Y. K. Mishra, D. K. Avasthi, D. Kabiraj, J. Ghatak and S. Varma, *Appl. Phys. Lett.*, 2008, 92, 103105.

7 H. Guo, W. Wang, L. X. Liu, Y. B. He, C. P. Li and Y. P. Wang, *Green Chem.*, 2013, 15, 2810–2816.

8 S. S. Chee and J. H. Lee, *J. Mater. Chem. C*, 2014, 2, 5372–5381.

9 A. Jaiswal, P. K. Gautam, S. S. Ghosh and A. Chattopadhyay, *J. Nanopart. Res.*, 2014, 16, 2188–738.

10 Y. X. Wang, H. Q. Sun, H. M. Ang, M. O. Tadé and S. B. Wang, *J. Colloid Interface Sci.*, 2014, 433, 68–75.

11 M. Ray, T. S. Basu, N. R. Bandyopadhyay, R. F. Klie, S. Ghosh, S. O. Raja and A. K. Dasgupta, *Nanoscale*, 2014, 6, 2201–2210.

12 X. L. Zhang, M. L. He, J. H. Liu, R. Liao, L. Q. Zhao, J. R. Xie, R. J. Wang, S. T. Yang, H. F. Wang and Y. F. Liu, *Chin. Sci. Bull.*, 2014, 27, 3406–3412.

13 J. Y. Sun, T. Gan, K. L. Wang, Z. X. Shi, J. J. Li and L. L. Wang, *Anal. Methods*, 2014, 6, 5639–5646.

14 Y. X. Zhang, M. Dong, S. J. Zhu, C. P. Liu and Z. Q. Wen, *Mater. Res. Bull.*, 2014, 49, 448–453.

15 Y. Zhang, C. S. Xing, D. L. Jiang and M. Chen, *Crystengcomm*, 2013, 15, 6305–6310.

16 V. Pilar, S. R. María Joséand and H. C. Manuel, *Talanta*, 2006, 69, 1063–1067.

17 X. M. Sun and Y. D. Li, *Langmuir*, 2005, 21, 6019–6024.

18 K. Wang, X. L. Zhang, C. Y. Niu and Y. Q. Wang, *ACS Appl. Mater. Interfaces*, 2014, 6, 1272–1278.

19 S. X. Mao, Y. M. Long, W. F. Li, Y. F. Tu and A. P. Deng, *Biosens. Bioelectron.*, 2013, 48, 258–262.

20 Y. Ma and Q. Zhang, *Appl. Surf. Sci.*, 2012, 258, 7774–7480.

21 M. Khan, C. S. Wei, M. M. Chen, J. J. Tao, N. D. Huang, Z. M. Qi and L. B. Li, *J. Alloy. Compd.*, 2014, 612, 306–314.

22 E. Laviron, *J. Electroanal. Chem.*, 1974, 52, 355–393.

23 X. J. Zhao, Y. L. Du, W. C. Ye, D. B. Lu, X. H. Xia and C. M. Wang, *New J. Chem.*,

2013, 37, 4045–4051.

24 W. L. Qin, X. Liu, H. P. Chen and J. Yang, *Anal. Methods*, 2014, 6, 5734–5740.

25 M. Behpour, S. Masoum and M. Meshki, *RSC Adv.*, 2014, 4, 14270–14280.

26 H. Karimi–Maleh, M. Moazampour, A. A. Ensafi, S. Mallakpour and M. Hatami, *Environ. Sci. Pollut. Res.*, 2014, 21, 5879–5888.

27 C. Y. Yang, S. M. Chen, T. H. Tsai and B. Unnikrishnan, *Int. J. Electrochem. Sci.*, 2012, 7, 12796–12807.

28 M. Moniruzzaman, I. Rodríguez, M. Ramil, R. Cela, S. A. Sulaiman and S. H. Gan, *Talanta*, 2014, 129, 505–515.

29 M. G. Scoralik, E. Daemon, C. M. D. Monteiro and R. Maturano, *Parasitol. Res.*, 2012, 110, 645–648.

30 S. Mishra and R. C. Sihag, *J. Apic. Sci.*, 2010, 54, 21–34.

31 F. X. Hu, Y. P. Bai and Y. Zhang, *J. Xinyang Normal Univ. (Natural Science Edition)*, 2009, 4, 561–564.